A&A 425, 143–149 (2004)
DOI: 10.1051/0004-6361:20041005

Astronomy & Astrophysics

Photoionization model analysis of the planetary nebula Hu1-2⋆

S. Hyung[1], S. R. Pottasch[2], and W. A. Feibelman[3]

[1] School of Science Education (Astronomy), Chungbuk National University, 48 Gaeshin-dong Heungduk-gu, CheongJu, ChungBuk 361-763, South Korea
e-mail: hyung@chungbuk.ac.kr
[2] Kapteyn Astronomical Institute, PO Box 800, 9700 AV Groningen, The Netherlands
[3] Laboratory for Astronomy and Solar Physics, Code 681, Goddard Space Flight Center, Greenbelt, MD 20771, USA

Received 1 April 2004 / Accepted 9 June 2004

Abstract. We have obtained high resolution optical spectra of the planetary nebula Hu 1-2 in the wavelength region of 3700 Å–10 050 Å, with the Hamilton Echelle Spectrograph (HES) at Lick Observatory. Diagnostic analysis indicates that the nebular gas can be represented by inhomogeneous shells of electron density $N_\epsilon \simeq 4000$–$10\,000$ cm^{-3}, and a gas temperature of 12 000–18 000 K. Using the spherically symmetric photoionization model with appropriate abundances, we tried to accommodate the observed physical conditions and high electron temperatures. The chemical composition of the nebula was derived from calculations using a photoionization model which predicts the observed IUE, HES and ISO line intensities; and the composition was then compared to previous determinations. Model analysis confirms the semi-empirically determined abundance derivations carried out in earlier studies. He and N abundances are high, but those of C, O, Ne and S are very low.

Key words. ISM: abundances – ISM: planetary nebulae: individual: Hu 1-2

1. Introduction

The planetary nebula (PN) Hu 1-2 (PNG 086.5–08.8) is a butterfly-like object of about 6″ × 2″ in radio maps. It is classified as a Peimbert's type I, i.e. objects with highly enhanced helium and nitrogen abundances, probably evolved from massive progenitors (see Peimbert & Torres-Peimbert 1983).

We secured a high dispersion optical spectrum, from 3700 to 10 050 Å, with the Hamilton Echelle Spectrograph (HES) at the Lick Observatory. Pottasch et al. (2003, hereafter, Paper I) analyzed the ISO far infrared spectrum, combined with the IUE ultraviolet observations to find the nebular abundances. They also used some HES data to derive the abundances. In our high dispersion spectrum, the spectral profiles are well separated into double peaks, so the spectrum of each blue and red component must be investigated separately during the extraction of the diagnostic information, if possible. The photoionization (P-I) model construction would allow us to find even abundances for rare elements. In this study, we will investigate the PN physical conditions and the diagnostics, from the HES high dispersion spectra, with an appropriate P-I model. We will also derive the abundances of Hu 1-2, based on our modelling efforts, and compare them with the previously determined empirical abundances, and with the average PN or solar abundances. With a proper P-I model which best fits the observed line intensities, one can also get an effective temperature for the central star of the PN (CSPN), and thereby infer its evolutionary status. We will check whether the P-I model can represent the observed electron temperatures and densities. Table 1 gives some basic data for Hu 1-2.

Table 1. Some basic data for Hu 1-2 (PNG 086.5–08.8).

$\alpha = 21^{\rm h}33^{\rm m}8\overset{\rm s}{.}0$, $\delta = 39^\circ38'01''(2000)$	
Diameter $\simeq 5$–$8''$	
log $F(\mathrm{H}\beta) = -11.21 \pm 0.01$ [erg cm^{-2} s^{-1}] (observed)	
$F(\mathrm{H}\beta) = 2.22 \times 10^{-11}$ erg cm^{-2} s^{-1} (unreddened, see text)	
Radial velocity = $-9.0\pm$ 8.1 km s^{-1}	
Expansion velocity = 29.0 and 32 km s^{-1}	
	([O III] and [N II], respectively)
Central star: $m_V = 17.32$	
	$T(\star) = 125\,000$ K (this paper)

These data are from Acker et al. (1992), unless otherwise indicated.

2. Observations

The spectrum in the visual wavelength region has been taken with the Hamilton Echelle Spectrograph (HES) at the Coudé focus of the 3 m Shane telescope of Lick Observatory. The spectral data were taken at 3 positions, centered at positions ∼3″ north and ∼3″ south of the CSPN and at the center

⋆ Table 3 is only available in electronic form at http://www.edpsciences.org

Table 2. Observing log of Hu 1-2.

Date (UT)	Setup	Exp. (m)	Setup	Exp. (m)
		North		
1991 Aug. 31	S127	120	123	120
	S127	15		
1991 Sep. 1	S125	120	121	120
	S125	25		
1991 Sep. 2	S124	100	126	100
2001 Aug. 28, 11	2K	60		
		Center		
1992 Sep. 16	S121	120	127	30
1992 Sep. 17	S125	120	125	5
1992 Sep. 18	S123	120		
		South		
1991 Aug. 30	S121	120	121	10
1991 Aug. 31	S127	15	125	6

Although the large 2048 × 2048 pixel CCD observation in 2001 covered the whole HES echelle pattern, the earlier smaller CCD chip required several settings (see text).

of the image, with a small 800 × 800 pixel CCD (on 1991 Aug. and Sep., 1992 Sep.); and these were supplemented by a large 2048 × 2048 pixel CCD observation (on 2001 Aug.). The sky was clear during our observations, and seeing was typically ∼1.5″ in 1991 and 1992, and ∼0.8″ in 2001. The 2001 observation was carried out only at the north position of the PN image. The slit entrance employed was ∼1.2″ × 4″ in image size at the Coudé focus, and it was placed at the center of the nebula. The spectral resolution limited by this slit size was about 2 pixels on the CCD chip, which amounted to 0.05 Å wavelength dispersion at 3600 Å, and increased to 0.15 Å at 8850 Å. The observations with the 800 × 800 pixel CCD chip required 6 setups, i.e. S124, S125 and S126 for the long wavelengths; S121 and S123 for the short wavelengths; and S127 for the middle wavelengths, to obtain Hα, [O III] and Hβ with one chip setting. 100 and 120 min long exposures are necessary to detect faint lines, while 15 and 25 min short exposures are required to avoid possible saturation effects in strong lines. The 2001 observation was done with a large 2048 × 2048 (2K) pixel CCD, which covered the whole echellogram in a single exposure. More details of the spectrograph used are described in Hyung (1994). We summarize the exposures in Table 2.

For data reduction, we also took exposures of a Th-Ar arc lamp to set the wavelength dispersion scale; a dome-quartz lamp to fix a flat field, which allowed us to correct for pixel-to-pixel sensitivity fluctuations; and finally exposures on standard stars of known energy distribution, i.e. HR 7596 and HR 9087. The reduction procedures are described in Hyung (1994). About 80 strong lines of the Hamilton Echelle data were already presented in Paper I, and these were studied together with the ISO data to derive abundances using the Ionization Correction Factor (ICF) method. In Table 3, we list a fuller set of the normalized line intensities. About 80 additional weak intensity lines are listed. The line intensities are given on the scale of $I(4861) = 100.0$, corrected for interstellar extinction, with an extinction coefficient $C = 0.60$. Some lines, e.g. N III 4640.66 and He I, are newly measured, but most of the lines also found in Paper I have the same intensity values. Columns 1 and 2 of Table 3 list the measured wavelength (corrected for radial velocity) and the ion. By comparing the observed wavelength, we can find the radial velocity of the nebula as follows: since most spectral lines are separated into double peaks, we derive the radial velocity by averaging the values found for the blue and red components at each slit position: (1) -1.54 km s^{-1} for the CSPN position (from -30.71 ± 0.92 (blue) and 27.64 ± 0.83 km s^{-1}(red)); (2) -4.39 km s^{-1} for the north position (from -32.44 ± 0.97 (blue) and 23.67 ± 0.91 km s^{-1}(red)). These values were obtained from a comparison of the observed wavelengths of the strong lines (I(lines) > 1.0) with the laboratory wavelengths, using the least squares method. From the above values, we adopt the CSPN slit position value, i.e. -1.54 ± 0.88 km s^{-1}, as the radial velocity of the PN, whereas Acker et al. (1992) quoted -9.0 ± 8.1 km s^{-1}. This discrepancy is perhaps caused by the slit positions being different. Column 3 gives the large CCD chip data for 2001, while Cols. 4–9 give the earlier smaller CCD chip data. Since most lines are well separated into the red (R) and blue (B) Doppler-shifted peaks, we list separately the combined, the red, & the blue components, i.e. $I(R + B)$, $I(R)$ and $I(B)$, respectively, all on the scale of $I(4861) = 100.0$. The extinction coefficient $C = 0.60$ was found from Balmer line ratios, such as $F(\mathrm{H}\alpha)/F(\mathrm{H}\beta)$, and from a comparison of Balmer and Paschen lines of the same upper quantum number. Fuller discussions on the earlier derivations of C can be found in Paper I. In Table 3 we have given 1 or 2 more significant figures than the data justify, to avoid round-off errors.

3. Nebular diagnostics

In Paper I, the electron density and temperature were found from the combined data set of *IUE*, optical and ISO data. Most of the optical line profiles in Table 3 show a double peak feature, which will allow us to find the physical condition, electron density and temperature for the approaching and receding shells, from the blue and red line components. Separate analysis of these components might provide more accurate physical information for the PN.

Figure 1 shows the diagnostics based on the line ratios involving equivalent p^2 and p^4 electrons. Electronic collision strengths involving the plasma and nebular diagnostics are constantly updated from the most recently available data, as in our previous investigations, e.g. Hyung et al. (2001). The first two figures are for the north slit position: the electron densities are in the range $10^{3.6}$–$10^{4.0}$ cm^{-3} or 4000–10 000 cm^{-3}, but the electron temperatures are strongly scattered. It seems that the lines of high ionization potential are formed in the extremely high temperature region. The diagnostics obtained from the blue line profiles, Fig. 1b, appear to be more complicated or highly scattered than those from the red line profiles: the physical condition of the approaching region of the shell is perhaps more complicated and inhomogeneous than the receding region for the central slit position.

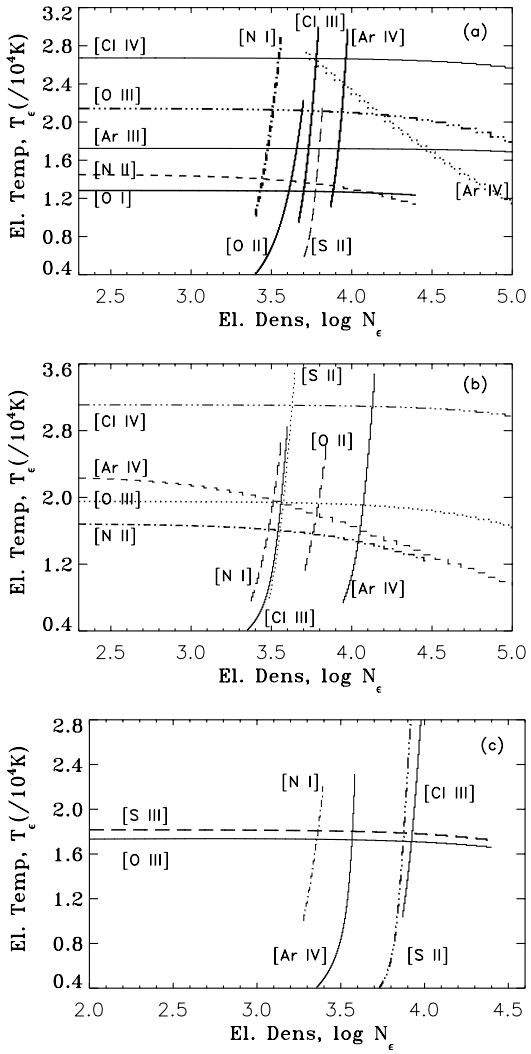

Fig. 1. Diagnostics showing T_ϵ and N_ϵ. **a)** Red profile or receding shell component of North; **b)** blue profile or approaching shell of North; **c)** red profile of Center.

There is not much diagnostic information, due to an incomplete observation at this position. Figure 1c shows the diagnostics obtained from the red line profiles, for the center position. Diagnostics of most ions do not converge at any special point. According to Aller & Liller (1968: see their Fig. 1), the He II4686/Hβ ratio ~0.88 implies that this PN has excitation class 4, and the line ratio $I(\lambda5007{+}4959)$/I(Hβ) indicates excitation class 5.5. The electron temperatures of the high excitation lines are extremely high, though. The nebula appears to consist of many inhomogeneous blobs and filaments, and it would be interesting to check whether the P-I model, without shock heating contribution, could produce the precise physical conditions of the shell. Some effects of T_ϵ fluctuation may also exist (see Peimbert et al. 1995).

3.1. Electron density

Table 4 lists line ratios suitable for fixing the electron density, N_ϵ. The lines are arranged roughly from low to high excitation. The ions and the wavelengths of the lines used to determine

Table 4. Line ratios suitable for fixing N_ϵ.

Ion	Lines used	Ratio (R)	Ratio (B)	log N_ϵ (R, B)†
	North			
[N I]	5198/5200	1.53	1.54	(3.5, 3.5)
[S II]	6731/6716	1.77	1.57	(3.8, 3.6)
[O II]	3726/3729	2.05	2.19	(3.7, 3.8)
[Cl III]	5538/5518	1.38	1.19	(3.7, 3.6)
[Ar IV]	4740/4711	1.38	1.60	(3.9, 4.1)
	Center			
[S II]	6731/6716	1.83	2.13	(3.9, ?)
[Cl III]	5538/5518	1.66	1.15	(3.9, 3.5)
[Ar IV]	4740/4711	1.04	0.869	(3.5, 3.5)

(R) and (B): red and blue components, respectively. † log N_ϵ(cm^{-3}) at T_ϵ = 17 000 K. "?" means out of range.

N_ϵ are listed in the first two columns, while the observed line intensity ratios are given in Cols. 3 and 4, for the receding and approaching components, respectively; and finally the derived number densities, log N_ϵ, are given in the last column; these values are derived assuming an electron temperature of T_ϵ = 17 000 K (see Table 5). More precise values can, of course, be found from Fig. 1. Although there is no indication of any systematic difference between the rear receding and the front approaching shells, the electron density appears to be in the range between 4000 and 10 000 cm^{-3}, with one exception of $N_\epsilon \simeq$ 12 500 cm^{-3} in (Ar IV). If we examine the spectral data of the northern blob only, the density of the high excitation lines appears to be slightly higher than that of the low excitation lines (see Figs. 1a and b). Since the data did not cover the full wavelength range for the central region, there are not very many lines in this region (see Fig. 1c). We will use a density of 5000 cm^{-3} in deriving the electron temperature in the next section.

3.2. Electron temperature

A number of ions sensitive to the electron temperature are listed in Table 5. The successive columns list the ions, the lines used, the corresponding intensity ratios for the red and blue components, and finally the electron temperatures derived. As in Table 4, we list the ions roughly in order of increasing ionization stages, and the electron temperatures are derived with the above-mentioned density, N_ϵ = 5000 cm^{-3}. The electron temperatures appear to increase roughly as a function of ionization potential. This result agrees with the derivation in Paper I. The electron temperatures of most other ions are extremely high, viz. above 17 000 K. Similar results are found from the ISO line spectrum (see Paper I). As pointed out in Paper I, the two ions with low ionization potential, O I and N II, which might be formed in the outer regions, show lower electron temperatures, but they are still high compared to those in other PNs, i.e. 13 000–15 000 K. We examine whether the ordinary photoionization model can predict these much higher electron temperatures.

Table 5. Line ratios suitable for fixing T_ϵ.

Ion	Lines used	Ratio (R)	Ratio (B)	$T_\epsilon/10^3$K (R, B)[†]
	North			
[O I]	6300/5577	52.5	–	(12.7, –)
[N II]	(6548+6584)/5755	39.3	31.2	(13.7, 15.8)
[Ar III]	(7751+7136)/5192:	50.9	23.6	(17.2, -?-)
[O III]	(4959+5007)/4363	35.4	41.2	(21.3, 19.3)
[S III]	9069/6312[‡]	4.06	4.75	(-?-, 29.9)
[Ar IV]	(4740+4711)/7171:	32.9	44.3	(26.5, 18.7)
[Cl IV]	8046/5324:	5.73:	5.18:	(26.7, 31.0)
	Center			
[N II]	(6548+6584)/5755	12.9	12.2	(-?-, -?-)
[O III]	(4959+5007)/4363	52.7	16.5	(17.2, -?-)
[S III]	9069/6312[‡]	7.71	6.11	(18.0, 22.2)
[Cl IV]	8046/5324:	4.71	6.07	(-?-, -?-)

[†] Temperature found assuming $N_\epsilon = 5000$ cm^{-3}. The colon (:) means lines with low intensities are involved. "-?-" means out of range, or too high. [‡] Uncertain due to Hα drip correction.

Table 6. Model details for Hu 1-2.

Parameter	Model
$R_{\rm in}$	0.017 pc
$R^a_{\rm out}$	0.024 pc (∼3.25″)
$N_{\rm H}$	6300 cm^{-3}
DISTANCE	1500 pc
$M_{\rm dust}/M_{\rm gas}$	0.001
F(Hβ)–obs[b] ≃	2.45(−11) erg cm^{-2} s^{-1}
F(Hβ)–pred	2.65(−11) erg cm^{-2} s^{-1}
CSPN $T(\star)$[c]	125 000 K (log g = 5.3)
$R(\star)$	0.056 $R_\odot$ ($L(\star)$ = 700 $L_\odot$)
T_ϵ([O II, III, IV])	14 200, 15 300, 16 600 K
Magnitude	$V^d_{\rm obs}$ = 16.05–16.50 and $V_{\rm pred}$ = 16.03

[a] Density bounded. [b] Extinction corrected with $C = 0.6$. [c] Hubeny non-LTE model atmosphere. See text. [d] Corrected with $E(B-V) = 0.41$ (or $C = 0.60$).

4. Abundance derivation with theoretical models

4.1. Theoretical models

The distance of Hu 1-2 is not known, although most values given in the literature range between 1 and 2 kpc. Recently, Hajian & Terzian (1996) gave a lower limit of 1.17 kpc, based on radio imaging. As in Paper I, we shall adopt a distance of 1500 pc.

The P-I code used here is that of Hyung (1994). It was originally made for studying the PN line intensities for bilaterally symmetrical compact objects, see e.g. Hyung & Aller (1996). Here, we do not employ an axi-symmetric model geometry, since the nebular image is relatively large and the simple spherically symmetric model seems to fit the observed (slit entrance) line intensities fairly well. To construct a theoretical model, one must know the spectral energy distribution (SED), or else certain other properties, of the CSPN. The SED of the CSPN can be calculated employing a model atmosphere. The hydrogen Zanstra temperature $T_{\rm z}$(H) is about 100 000, K and the ionized helium Zanstra temperature $T_{\rm z}$(He II) is about 145 000 K (see Paper I). In Paper I, $T_{\rm star}$ = 140 000 K is the most probable temperature to explain various high excitation lines in the nebula. We directly applied Hubeny's theoretical model atmospheres (Hubeny 1988), based on some of the selected properties of the CSPN, i.e. $T_{\rm eff}$, stellar radius, and log g, to the photoionization modelling, until it gave a correct level of nebular excitation (using the energy-balance method and the Zanstra method), and the correct electron temperatures. From our trials, we found that model atmospheres with relatively high temperatures are suitable for the CSPN, e.g. $T_{\rm eff}$ = 125 000 K. The P-I model predictions with a lower temperature model atmosphere, e.g. $T_{\rm eff}$ ∼ 100 000 K, or higher temperature, e.g. $T_{\rm eff}$ ∼ 145 000 K, were not satisfactory. The CSPN energy distribution used in the model has $T_{\rm eff}$ = 125 000 K, and log g = 5.3, with He/H = 0.13, and with a nebular heavy element distribution in the central star. In Fig. 1, the electron number density is $N_\epsilon \sim$ 4000–10 000 cm^{-3}. The nebula is assumed to be a homogeneous shell with $N_{\rm H}$ = 6300 (or $N_\epsilon \sim$ 7500) cm^{-3}. No filling factor was introduced in the shell gas. We assume a central star radius of $R_* = 0.056\ R_\odot$, and, as a result, $L_* = 700\ L_\odot$. We assumed only a small value for the dust-to-gas ratio, $M_{\rm dust}/M_{\rm gas}$ = 0.001.

The details of the parameters adopted in our model are given in Table 6. For an assumed distance of 1.5 kpc, we calculate the CSPN properties and the absolute Hβ flux. Acker et al. (1992) quoted a visual magnitude for the CSPN of m_v = 17.32, while Heap et al. (1990) measured it to be m_v = 17.76; from this, the intrinsic visual magnitudes are $V_{\rm obs}$ = 16.05–16.50, with C = 0.60 (or E_{B-V} = 0.41, and the corresponding total extinction $A_{\rm v}$ is taken as $3.1E_{B-V}$). The model predictions give values that are about one magnitude lower than the observed ones: $V_{\rm pred}$ = 16.03 and $B_{\rm pred}$ = 15.73. The outer shell boundary is slightly smaller than the observed nebular optical image radius. To fit the observed outer boundary size, we must introduce a filling factor, which was not done.

Table 7 compares the observed and predicted intensities. Intensities for the CSPN and north blob positions obtained in 1991 and 1992 are given in Cols. 3 and 4, respectively, while the north position 2K CCD data taken in 2001 are given in Col. 5. The *IUE* Archive and ISO intensities are calculated using the flux data taken from Paper I (see their Tables 1 and 3), which are also listed in square brackets or parentheses in Col. 4. Column 6 lists the predicted intensities, and all of the values are given on a scale of I(Hβ) = 100.

For most ions, fairly reasonable agreement between the observed and predicted intensities is achieved; but in some cases, especially the weakly detected *IUE* lines, e.g. N IV] and N IV], we find a large discrepancy. As usual, we properly treated collisionally excited contributions in predicting the He lines. The agreement for He I and He II seems to be fine.

Table 7. Comparison of observed and predicted intensities.

El–ion	λ	I(C)	I(N)	I(N-2K)	I(Model)
He I	5876	11.51	10.06	7.35	9.33
	6678	–	2.44	2.41	2.09
	4471	3.85	2.68	3.23	3.35
He II	4686	88.76	73.84	81.34	83.71
	5412	5.44	5.95	7.13	7.20
	1640		[604]		632
C II	2325/28		[83.8]		54.7
	4267		–		0.09
C III	1907/09		[441]		560
C IV	1548/51		[712]		505
N II	6584	241.7	171.1	136.3	158.6
	6548	71.76	58.96	40.98	54.75
	5755	5.67	5.67	4.42	6.02
N III	1747–52		[171]		134
N IV	1483/86		[256]		91.7
N V	1239/42		[243]		28
O I	6300	–	6.67	5.59	0.14
	6363	2.81	2.12	2.07	0.05
O II	3726	–	31.94	30.54	29.31
	3729	14.94	15.45	14.42	12.68
	7321/2	4.24	–	4.55	3.91
	7332/3	3.18	–	3.97	3.13
	7321/2	–	–	4.55	3.91
	7332/3	–	–	3.97	3.13
O III	1660/66		[45]		39
	4363	24.57	25.65	19.19	14.86
	4959	279.0	221.4	224.4	254.1
	5007	823.3	717.0	745.7	731.9
O IV	1397–1407		[57]		14
Ne III	3868	86.90	70.27	68.67	81.62
	3968	27.57	26.37	25.83	24.36
Ne IV	2422/25		[213]		50
	4725/27	2.23	2.96	–	0.53
Ne V	3426		(181)		14.47
S II	4068	3.41	3.30	2.99	1.48
	4076	0.99	1.19	–	0.50
	6717	6.17	5.42	4.78	1.30
	6731	11.92	11.02	7.47	2.39
S III	6312	2.14	3.48	3.24	1.88
	9069	14.86	13.38	12.26	18.96
	9531	36.97	21.54	25.24	46.20
S IV	10.5 μm		(50.8)		51.98
Cl II	8579	–	0.16	–	0.17
Cl III	5518	0.50	0.48	–	0.49
	5538	0.71	0.59	0.59	0.78
Cl IV	7530	0.48	0.46	–	0.35
	8046	0.84	0.87	0.90	0.87
Ar III	5192	0.25	0.29	–	0.20
	7136	11.81	10.96	9.63	12.86
	7751	–	2.18	2.67	3.11
Ar IV	4711	5.65	4.25	5.76	4.40
	4740	5.45	6.51	6.26	5.92
	7238	0.37	0.37	–	0.16
	7263	–	0.31	–	0.18
	7171	–	0.28	–	0.22
Ar V	6435	–	1.32	1.86	1.28
	7005	–	2.69	4.16	2.74
Ca V	5310	0.13	0.08	0.17	–
K IV	6102	0.30	0.30	0.35	–
Si III	1883/92		[37]		36.5

I(C): slit position at the CSPN position. I(N): slit at the north of the CSPN. I(N-2K): 2001 2K-data. Intensities in square brackets and parentheses are from Pottasch et al. (2003).

The predictions for C also seem to be fine, except for the recombination C II λ4267 line, and C IV. Simultaneously fitting the optical and *IUE* nitrogen line intensities with the P-I model seems to be impossible. There may be an unavoidably large error involved in the *IUE* line intensities: it could be due to measurement uncertainty, or to an overestimated extinction correction. Here, our model predictions are consistent with the optical lines.

Predictions for the ions of O, Ne, S, Cl and Ar seem to be generally successful. The prediction for the [O I] and [S II] lines, which might have formed in or near the neutral cloud region, indicate some problem, though. However, the agreement for oxygen and sulfur lines, including the [S IV] ISO IR line, appears to be fine. Rare elements like Ca, K, and Si are all represented by single ionization stages: calcium by [Ca V], potassium by [K IV], and silicon by Si III]. Hence, agreement for these ions can be assured, and the abundances of these elements can be found from the model.

The diagnostic electron temperatures are $T_\epsilon \sim 15\,000$, 17 000 K and 20 800 K, for [N II], [Ar III] and [O III], respectively (see Fig. 1a and Table 5), while the model predicts $T_\epsilon \simeq$ 14 200 K, 15 900 K and 16 600 K, respectively; and it gives $T_\epsilon \simeq 14\,200$ K and 15 300 K, for [O II] and [O IV], respectively. The photoionization model cannot predict the large scatter indicated by the diagnostics. The relatively higher temperatures implied by the diagnostics in [O III], [Ar IV] and [Cl IV] are obviously not confirmed by the model. We do not have a reliable way of estimating the error, but there could be other factors or physical mechanisms involved, such as shock heating which may have contributed to the excitation of lines. Since our model structure is an idealized, simple, homogeneous shell, it does not admit a point-to-point fluctuation of N_ϵ and T_ϵ. Nonetheless, our photoionization model broadly reproduces the observables. It gives a reasonable effective temperature for the CSPN, similar to derivations by other methods. The CSPN temperature of Hu 1-2 is likely to be around $T_{\rm eff} = 125\,000$ K, similar to that of IC 5117 (see Hyung et al. 2001).

4.2. Elemental abundances

Table 8 compares the abundances derived in this paper with earlier values found in Paper I and in the literature. The earlier abundance determinations are mostly obtained from an Ionization Correction Factor (ICF) method. See Paper I for detailed information on these earlier derivations. If we compare our model abundances with the semi-empirical derivation of Paper I, there is a fairly good agreement for He, C, N, Ar and Cl, i.e. to within 10%, while the currently derived O, S and Ne abundances are 17–40% lower than those of Paper I. The helium abundances in both this paper and Paper I, are lower than those in Aller & Czyzak (1983) or Malkov (1998). We adopt 0.13 as the relative helium abundance. Compared with the earlier studies, the uncertain ICF was very small in Paper I, usually less than a factor 1.5, so the elemental abundances of Paper I are probably the best-determined. Thus, if the present value is close to that in Paper I, we adopt the Paper I value as a recommended elemental abundance relative to H^+,

Table 8. Comparison of abundances in Hu 1-2.

El.	Present	Paper I	AC(1)	Malkov(2)	PT(3)
He	0.130	0.127	0.158	0.154	0.147
C(−4)	1.6	1.62	1.2	1.2	
N(−4)	1.7	1.9	3.2	1.5	2.2
O(−4)	1.3	1.57	1.1	1.1	1.6
S(−6)	3.0	4.2	3.0	7.8	3.1*
Ar(−6)	1.2	1.1	1.6	0.87	0.79
Ne(−5)	3.0	4.9	6.7	5.9	3.6
Cl(−7)	1.2	1.1	1.5		
Ca(−8)	9.0				
K(−8)	9.0				
Si(−6)	5.0				

(1) Aller & Czyzak (1983); (2) Malkov (1998); (3) Peimbert & Torres-Peimbert (1995); * Sabbadin et al. (1987).

Table 9. Comparison of abundances in Hu 1-2.

Element	Hu 1-2	PN Ave.[a]	Sun[b]
He	0.13	0.11	0.086
C(−4)	1.6	6.48	2.57
N(−4)	1.8	1.4	0.63
O(−4)	1.3	4.93	4.57
Ne(−5)	4.9	12.5	6.92
S(−6)	3.5	8.08	21.4
Ar(−6)	1.1	2.42	1.51
Cl(−7)	1.1	1.66	3.16
K(−8)	9.0		13.2
Si(−6)	5.0		35.5
Ca(−8)	9.0		229

[a] Average (or normal) abundances from Kingsburgh & Barlow (1994) and Aller & Czyzak (1983). [b] Solar abundances are from Christensen-Dalsgaard (1998) for He; Asplund (2003) for C & N; Asplund et al. (2004) for O, Ne & Ar; and Grevesse & Sauval (1998) for others, respectively.

$N(\mathrm{el})/N(\mathrm{H}^+)$. The values are 1.6(−4) for C; 1.8(−4) for N; 1.1(−6) for Ar; and 1.1(−7) for Cl, respectively. For other uncertain cases, we adopt the mean value from the two papers, but sometimes we chose the value close to either the present model, or to the Paper I value, in the case where derivations from other sources are much closer to one of them, i.e. 1.3(−4) for O; 4.9(−5) for Ne; and 3.5(−6) for S.

5. Conclusions

Table 9 compares the Hu 1-2 abundances with the average PN abundances by Aller & Czyzak (1983) and by Kingburgh & Barlow (1994), and with the solar abundances given in the literatures. Of a number of nebulae whose ICF abundances had been determined with the high dispersion spectroscopic or ISO measurements, Hu 1-2 has the lowest abundance yet found (see Paper I). He and N are exceptions. Except for these two elements, the abundances are even lower than the solar values. The presently derived values for the model are even slightly lower than those in Paper I.

The lower abundances of carbon, oxygen, neon, sulfur and argon, which are not produced in the CSPN in the course of its evolution, and instead reflect the abundances in the star at the time of its formation, suggest that Hu 1-2 is much older than the other PNs observed. As mentioned in Paper I, it also indicates that the CSPN progenitor must be a low mass star, and, as a result, its evolution should have proceeded much more slowly. Meanwhile, a higher abundance of nitrogen and an enhanced abundance of helium, which must have been formed in the course of the evolution of the central star, suggest that it may have been of high mass ($\geq$2.4 $M_\odot$ according to Peimbert & Torres-Peimbert 1983). Since all the other elemental abundances are very low, it has perhaps not evolved from such a high mass star. Hu 1-2 may still be classified as a Peimberts' type I, though, in view of the enhancement of the He and N abundances.

It would be interesting to see what would be the CSPN mass, based on the current model: taking $L(\star)$ and $T(\star)$ at their face values (see Table 6), and utilizing Schönberner's (1983) and Vassiliadis & Woods (1994) evolutionary tracks, we find a CSPN mass of about 0.56 $M_\odot$. In addition, these evolutionary tracks suggest a corresponding age of about 22 000 years, for the evolution from the AGB progenitor phase. We employed the spherically symmetric P-I model to study the spectra secured from the UV-optical-IR wavelength region. The P-I model constructed in this paper, gives a fairly good representation of the observed physical conditions of Hu 1-2. It confirms that the lower abundances, except for He and N, are the main cause of the extremely high electron temperatures found in this object. In its main sequence phase, the progenitor star must have been slightly less massive than our Sun, which confirms the Paper I result. As indicated in Paper I, Hu 1-2 could have evolved from a star which had been formed earlier in the history of the evolution of our Galaxy. The Hu 1-2 YSO progenitor might have been formed in a chemically uncontaminated region of the Galaxy, e.g. near the Galactic halo.

Acknowledgements. We express our gratitude to the late Prof. Lawrence H. Aller (UCLA) for his support of this work. He worked with one of the authors, S.H., but unfortunately passed away before he could review a draft of this paper. We thank Dr. André B. Fletcher (Korea Astronomy Observatory) for his proof-reading and Dr. Silvia Torres-Peimbert (UNAM) for her careful review and valuable comments. We are also thankful to the technical staff of Lick Observatory, who helped us secure the Hamilton Echelle data. This work was the result of research activities of the Astrophysical Research Center for the Structure and Evolution of the Cosmos (ARCSEC), supported by the Korea Science & Engineering Foundation.

References

Acker, A., Ochsenbein, F., Stenholm, B., et al. 1992, Strasbourg-ESO Catalogue of Galactic Planetary Nebulae, Garchung bei Munchen, European Southern Observatory

Aller, L. H., & Czyzak, S. J. 1983, ApJS, 51, 211 (AC83)

Aller, L. H., & Liller, W. 1968, in Nebulae and Interstellar Matter, ed. B. M. Middlehurst, & L. H. Aller (Chicago: University of Chicago Press), Chap. 9, 498

Asplund, M. 2003, in CNO in the Universe, ed. C. Charbonnel, D. Schaerer, & G. Meynet, ASP Conf. Ser., 304, 275

Asplund, M., Grevesse, N., Sauval, A. J., et al. 2004, A&A, 417, 751

Christensen-Dalsgaard, J. 1998, Space Sci., 85, 19

Grevesse, N., & Sauval, A. J. 1998, Space Sci. Rev., 85, 161

Hajian, A. R., & Terzian, Y. 1996, PASP, 108, 258

Heap, S. R., Corcoran, M., Hintzen, P., & Smith, E. 1990, From Miras to PN, ed. M. O. Mennessier, & A. Omont (Gif-sur-Yvette: Éditions Frontières)

Hubeny, I. 1988, Computer Phys. Comm., 52, 103

Hyung, S. 1994, ApJS, 90, 119

Hyung, S., Aller, L. H., Feibelman, W. A., & Lee, S.-J. 2001, ApJ, 563, 889

Kingsburgh, R. L., & Barlow, M. J. 1994, MNRAS, 271, 257

Malkov, Yu. F. 1998, A. Rep., 42, 293

Peimbert, M., Luridiana, V., & Torres-Peimbert, S. 1995, RMxA&A, 31, 147

Peimbert, M., & Torres-Peimbert, S. 1983, IAU Symp., 103, 233

Pottasch, S. R., Hyung, S., Aller, L. H., et al. 2003, A&A, 401, 205 (Paper I)

Sabbadin, F., Cappellaro, E., & Turatto, M. 1987, A&A, 182, 305

Schönberner, B. 1983, ApJ, 272, 708

Vassiliadis, E., & Wood, P. R. 1994, ApJS, 92, 125

Online Material

Table 3. Optical Spectrum of Hu 1-2 (North & Center).

			North				Center	
λ_{obs}	Ion	$I(2001)$	$I(R+B)$	$I(R)$	$I(B)$	$I(R+B)$	$I(R)$	$I(B)$
3705.05	He I			1.01				
3711.87	H I			1.01				
3726.07	[O II]	30.54	31.94	39.12	12.38			
3728.83	[O II]	14.42	15.45	19.05	5.65	14.94	12.35	19.22
3734.33	H I		1.47	1.55	1.26			
3750.05	H I			2.20			2.32	
3759.79	O III		1.93	2.21	1.14	2.14	1.75	2.80
3797.83	H I			3.46		4.68	4.15	5.57
3819.61	He I		0.36					
3835.23	H I	6.79	5.30			6.66	5.82	8.04
3857.84	He II		0.37					
3862.32	Si II		0.29					
3868.74	[Ne III]	68.67	70.27	84.67	30.77	86.90	73.02	109.8
3888.68	He I	21.86				18.89		
3889.21	H I			3.42				
3964.75	He I			0.50		0.49	0.33	0.75
3967.45	[Ne III]	25.83	21.68	26.37	9.08	27.57	22.74	35.55
3970.01	H ϵ	16.97	11.55	12.29	9.48	16.24	14.91	18.45
4024.78	He II		0.34	0.31	0.40			
4026.22	He I (18)	2.33	1.79	1.57	2.36	1.06	0.94	1.25
4068.63	[S II]	2.99	3.30	4.00	1.41	3.41	2.74	4.52
4076.36	[S II]		1.19	1.41	0.59	0.99	0.70	1.46
4097.17	N III, O II			0.77		0.75	0.64	0.95
4099.87	He II		0.79	0.74	0.95	0.96		
4101.68	H δ	23.51	20.01	21.15	16.00	25.49	23.47	28.82
4103.30	N III		0.39	0.43	0.30			
4120.66	He I		0.28					
4143.76	He I		0.23	0.25	0.19			
4163.00	[K V]			0.16				
4199.66	He II	1.33	1.19	1.11	1.38	1.48	1.20	1.95
4227.41	[Fe V]		0.20	0.17	0.30			
4338.52	He II	3.19	2.34	2.17	2.82			
4340.43	H γ	43.58	49.13	48.79	49.81	48.19	47.49	49.37
4357.91	O II	1.43						
4363.16	[O III]	19.19	25.65	27.61	20.28	24.57	22.34	28.25
4387.93	He I		0.35	0.39	0.26			1.33
4471.51	He I	3.23	2.68	4.57	2.45	3.85	3.53	4.38
4541.43	He II	3.19	3.14	3.19	2.97	2.94	2.95	2.92
4571.22	[Mg I]		0.34	0.46	0.29	0.34	0.28	0.44
4606.12	Fe III		0.14	0.12	0.17			
4625.08	[Ar V]					0.54		
4634.09	N III		0.39	0.46	0.21	0.35	0.27	0.49
4640.66	N III	0.87	0.84	0.91	0.40	1.04	0.97	1.16
4641.79	O III, N III			0.02				
4647.35	C III		0.11			0.34		
4649.14	O II		0.04					
4651.05	O II		0.10					
4658.21	C IV, [Fe III]		0.22	0.21	0.24	0.28	0.28	0.29
4685.58	He II	81.34	73.84	74.52	71.66	88.76	87.65	90.60
4711.28	[Ar IV]	5.76	4.53	4.43	4.77	5.65	4.98	6.77
4714.15	[Ne IV]	1.02	1.40	0.84	3.02	0.80	0.81	0.79
4724.06	[Ne IV]		1.36	1.32	1.45	1.21	1.08	1.42
4725.47	[Ne IV]		1.61	1.52	1.86	1.02	0.83	1.33
4740.09	[Ar IV]	6.26	6.51	6.11	7.62	5.45	5.19	5.88
4859.08	He II		4.59	4.49	5.52	3.02		
4861.29	H β	100.0	100.0	100.0	100.0	100.0	100.0	100.0
4922.00	He I		0.90	1.38	0.75		0.99	
4931.28	[O III]		0.39	0.20	0.90			

Table 3. continued.

			North			Center		
λ_{obs}	Ion	$I(2001)$	$I(R+B)$	$I(R)$	$I(B)$	$I(R+B)$	$I(R)$	$I(B)$
4958.99	[O III]	244.4	221.4	241.6	166.4	279.0	303.5	238.5
4972.14	[Fe VI]		0.20					
4987.98	[Fe VII]		0.14					
5006.88	[O III]	745.7	717.0	735.4	669.2	823.3	874.6	738.6
5015.81	He I	1.21	2.24	2.42	1.71	1.63	1.62	1.65
5017.56	†	0.57	0.71	0.71	0.74	0.40	0.28	0.60
5047.92	He I		0.27	0.27	0.26			
5131.32	C III		0.23					
5145.51	[Fe VI]		0.20	0.09	0.22	0.19	0.13	0.29
5158.47	[Fe II,VII?]		0.25				0.25	
5191.78	[Ar III]		0.29	0.29	0.37	0.25	0.27	0.23
5198.10	[N I]	1.03	1.70	1.90	1.14	1.45	1.38	1.57
5200.47	[N I]		1.11	1.24	0.74	0.96	0.96	0.96
5270.58	[Fe III]		0.08					
5308.79	[Ca V]		0.17	0.20	0.16	0.08		
5323.05	[Cl IV]		0.11	0.15	0.17	0.16	0.17	0.15
5334.67	[Fe II]		0.14			0.19	0.14	0.29
5411.30	He II	7.13	5.95	6.44	5.34	5.44	5.98	4.54
5460.39	line?	0.69						
5517.73	[Cl III]		0.48	0.48	0.43	0.50	0.44	0.60
5537.89	[Cl III]	0.59	0.59	0.66	0.51	0.71	0.73	0.69
5577.18	[O I]			0.16				
5591.79	O III			0.17			0.19	
5592.06	O III		0.13	0.12				
5630.40	[Fe VI]		0.08					
5676.78	[Fe VI]		0.18					
5697.09	line?					0.21		
5720.52	[Fe VII]		0.35			0.31	0.31	0.31
5754.71	[N II]	4.42	5.67	7.22	2.82	5.67	6.12	4.93
5768.52	†					0.17		
5791.98	He II?					0.22		
5800.28	C IV		0.14					
5812.52	C IV		0.11					
5843.96	line?					0.06		
5846.26	He II					0.08		
5856.76	He II		0.10					
5875.75	He I	7.35	10.06	11.73	4.85	11.51	12.67	9.58
5881.95	He II		0.10					
5896.41	He II					0.28		
5913.13	He II		0.07					0.41
5931.27	N II					0.15		
5952.77	He II		0.21	0.15	0.30	0.13		
5976.63	He II		0.13	0.14		0.13		
6004.63	He II		0.12				0.21	
6036.36	He II		0.17	0.08		0.19		
6074.04	He II		0.18	0.20	0.24	0.23		
6086.16	[CaV]+[FeVII]		0.52				0.67	
6101.59	[K IV]		0.35	0.26	0.27	0.30	0.28	0.35
6117.88	He II		0.17	0.23	0.29			
6170.49	He II		0.23	0.17	0.16	0.22		
6227.68	[K VI]		0.23			0.10		
6233.49	He II		0.29	0.22	0.30		0.45	
6300.38	[O I]	5.59	6.67	8.49	1.69			
6310.99	He II				0.22			
6312.00	[S III]	3.24	2.76	3.48	2.37	2.14	1.80	2.70
6363.64	[O I]	2.07	2.12	2.72	0.84	2.81	2.80	2.82
6406.18	He II		0.34	0.40	0.41		0.61	
6434.56	[Ar V]	1.86	1.32	1.24	1.19			

Table 3. continued.

			North				Center	
λ_{obs}	Ion	I(2001)	$I(R+B)$	$I(R)$	$I(B)$	$I(R+B)$	$I(R)$	$I(B)$
6526.80	He II		0.41	0.41				
6527.25	[N II]				0.30			
6548.22	[N II]	40.98	58.96	70.89	27.52	71.76	78.81	60.12
6559.92	He II		10.88	10.85	10.95	14.72	16.66	11.51
6562.81	H α	281.4	268.1	275.6	247.4	334.7	349.4	310.4
6583.52	[N II]	136.3	171.1	213.0	60.49	241.7	256.3	217.4
6678.18	He I	2.41	2.44	3.05	0.77			
6682.91	He II		0.50	0.53	0.43			
6716.67	[S II]	4.78	5.42	6.21	3.25	6.17	6.57	5.50
6730.72	[S II]	7.47	9.42	11.02	5.11	11.92	12.05	11.70
6890.37	He II	0.97	0.75	0.68	0.56	0.76		
7005.27	[Ar V]	4.16	2.69	2.58	1.86			
7064.85	He I	4.08	5.10	6.07	2.44	6.37	6.61	5.98
7135.82	[Ar III]	9.63	10.96	12.15	7.70	11.81	12.10	11.34
7170.36	[Ar IV]		0.28	0.32	0.28			
7177.32	He II		0.58	0.59	0.54			
7237.31	[Ar IV]		0.37	0.38	0.49	0.37		
7262.72	[Ar IV]		0.31	0.31	0.30			
7281.33	He I		0.66	0.81	0.25			
7319.00	[O II]	4.55				4.24	5.75	1.66
7330.14	[O II]	3.97				3.18	2.93	3.58
7529.66	[Cl IV]		0.46	0.48	0.43	0.48	0.45	0.53
7592.39	He II	1.48	1.14	1.07	1.26	1.10	0.95	1.35
7751.01	[Ar III]	2.67	2.18	2.60	1.05			
8045.50	[Cl IV]	0.90	0.87	0.86	0.88	0.84	0.80	0.91
8236.38	He II	2.29	1.46	1.55	1.20			
8374.37	H I		0.21					
8391.62	H I		0.27					
8413.17	H I		0.31				0.23	
8467.17	H I		0.49					
8502.38	H I		0.58				0.53	
8543.86	H I		0.74	0.55	0.68		0.61	
8578.85	[Cl II]		0.16					
8598.14	H I	0.74						
8664.57	H I	0.87	0.88	0.94	0.71	0.75	0.75	0.75
8750.25	H I		0.65					
8862.53	H I		0.82					
9014.60	H I	1.39	0.98					
9069.04	[S III]	12.26	13.38	14.14	11.26	14.86	13.87	16.50
9227.98	He I	1.73	1.61	1.77	1.84	1.71	1.69	1.74
9344.09	He I	0.47	0.42					
9530.59	[S III]	25.24	21.54	24.67	12.98	36.97	33.48	42.72
9545.96	H I	1.75	0.94	1.02	0.54			
9547.26	H I					1.80	1.97	1.53
10048.95	H I	2.95	2.27	2.20	1.66			
10123.16	He II	15.25	9.78	11.22	5.86			

See Hyung (1994) for the identifications and references therein. Interstellar extinction-corrected intensities are all given on the scale of $I(\mathrm{H}\beta) = 100$ ($C = 0.60$). I(2001): intensities of the 2001 Aug observation (at North); $I(R)$ and $I(B)$ are intensities from the red and blue-shifted line profiles, respectively, while $I(R+B)$ are intensities combined from both these profiles.